Int. J. Heat Mass Transfer. Vol. 33, No. 12, pp. 2701–2720, 1990
Printed in Great Britain

0017–9310/90 $3.00 + 0.00

Calculation of turbulent convection between corotating disks in axisymmetric enclosures

C. J. CHANG, J. A. C. HUMPHREY† and R. GREIF
Department of Mechanical Engineering, University of California at Berkeley, Berkeley, CA 94720, U.S.A.

(*Received* 11 *July* 1989 *and in final form* 23 *January* 1990)

Abstract—A numerical investigation is conducted for the case of turbulent flow in the unobstructed space between a pair of centrally clamped coaxial disks corotating in a fixed axisymmetric enclosure. The finite difference procedure of Chang *et al.* (*J. Heat Transfer* **111**, 625–632 (1989)) is extended to include a standard two-equation (k–ε) model of turbulence in the core of the flow. A van Driest relation, that accounts for the effects of streamline curvature and wall shear on the energy-containing length scales, is used in conjunction with Prandtl's mixing length hypothesis to model the near wall flow. The set of equations is solved assuming a constant property, circumferentially symmetric, statistically stationary flow. This approach predicts mean velocity and heat transfer results that are in good agreement with time-averaged experimental data. The predictions reveal a flow that, in non-dimensional variables, tends to a limiting asymptotic state at high Reynolds numbers. In the absence of blowing a symmetrical pair of cross-stream eddies appear near the enclosure wall the rotation of which increases with increasing disk rotational speed. High rotational speeds, in excess of 2400 rpm in the configuration studied, and small disk separations induce large values of shear and temperature (due to viscous dissipation) in the vicinity of the enclosure wall. The flow and its heat transfer characteristics can be drastically altered by the combined effects of radial and axial blowing. Specifically, it is shown that axial blowing significantly reduces the shear and heat transfer at the curved enclosure wall.

1. INTRODUCTION

1.1. *The problem of interest*

ROTATING disk flows have been the subject of considerable attention, for fundamental as well as practical reasons. In this regard, for example, free-spinning disks have served as models for understanding geophysical and engineering phenomena and have been investigated extensively, both experimentally and theoretically [1]. We are concerned here with the flow of air that arises in the unobstructed space between a pair of centrally clamped, coaxial disks that are corotating in a fixed axisymmetric enclosure or shroud. This configuration is of special relevance to magnetic disk storage systems in the computer industry, and also finds important applications in rotating machinery.

Figure 1 illustrates the basic geometrical element of interest and defines the coordinate system and problem notation. It provides the side view of a pair of disks that are corotating at angular velocity Ω. As will be discussed, calculations (supported by measurements) for this configuration show that the circumferential component of motion sets up an outwardly-directed centrifugal force field that is opposed by an inwardly-directed force due to the radial pressure gradient. The pressure gradient displaces slow moving fluid from the enclosure wall region into the core of the flow, along the symmetry plane, while the centrifugal force drives fluid in the thin boundary layer adjacent to each disk towards the enclosure wall. The result is a cross-stream secondary flow, similar (but of opposite sense of rotation) to that observed in curved pipes and ducts. Nearer the hub, in the absence of imposed throughflows, the air motion approaches the condition of solid body rotation. Above a critical speed of rotation, instabilities and mean flow unsteadiness arise. At still higher rotational speeds, a transition from laminar to turbulent flow takes place at a critical location, R_c, between the hub and the shroud.

Little of the information that is available on free-spinning disks is applicable to confined corotating disks. This is mainly due to the presence of the fixed enclosure wall (or 'shroud') which imparts a dominant shearing action on the flow; a constraint that is absent in the free-spinning disk case but present in many systems of practical interest.

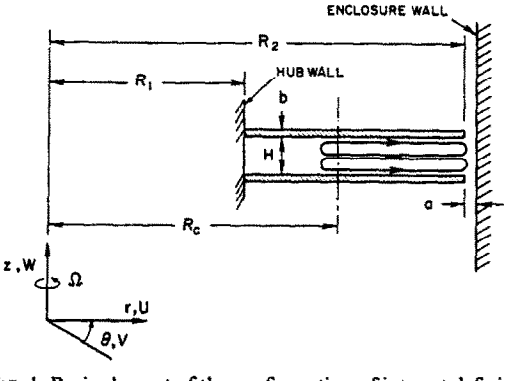

FIG. 1. Basic element of the configuration of interest defining variables and coordinate system notation. The origin of coordinates is located at the intersection of the axis of rotation and the geometrical symmetry plane between the two disks.

† Author to whom correspondence should be addressed.

NOMENCLATURE

A^+	constant in equation (11)
a	distance between disk periphery and enclosure wall
b	disk thickness
C_i	blowing parameter in radial ($i = r$) and axial ($i = z$) directions, $Q_i/\nu R_2$
C_p	specific heat at constant pressure
c_1, c_2, c_μ	model constants (see Table 1)
F	dimensionless shear stress (see equation (19))
f_1, f_2, f_μ	model functions (see Table 1)
H	distance between a pair of corotating disks
K	thermal conductivity
k	turbulent kinetic energy
l_m	curvature modified mixing length
l_0	van Driest mixing length (see equation (11))
Nu	Nusselt number (see equation (18))
P	pressure
Q_i	air volume flow rate in radial ($i = r$) and axial ($i = z$) directions
q_ω	heat flux at enclosure wall
R_1	hub radius
R_2	disk radius
R_c	critical radius for transition to turbulent flow
Ri	Richardson number (see equations (12) and (13))
Re	disk Reynolds number based on H, $\Omega R_2 H/\nu$
Re_r	disk Reynolds number based on R_2, $\Omega R_2^2/\nu$
r	radial coordinate direction
T	temperature
T_H	temperature of the hub
T_S	temperature of the enclosure wall or shroud
U	mean radial velocity component
u_τ	wall stress velocity, $\sqrt{\tau_\omega/\rho}$
V	mean circumferential velocity component
$\tilde{V}$	r.m.s. of circumferential velocity component
W	mean axial velocity component
y	wall coordinate
y^+	dimensionless wall coordinate, yu_τ/ν
z	axial coordinate direction.

Greek symbols

α_e	effective thermal diffusivity
β	constant in equation for l_m
δ	boundary layer thickness
ε	dissipation of turbulent kinetic energy
θ	circumferential coordinate direction
κ	von Karman constant
λ_k	effective diffusivity for k
λ_ε	effective diffusivity for ε
μ	dynamic viscosity
ν	kinematic viscosity
ν_e	effective kinematic viscosity, $\nu + \nu_t$
ν_t	turbulent kinematic viscosity
ρ	density
σ_k	turbulent Prandtl number for k
σ_T	turbulent Prandtl number for T
σ_ε	turbulent Prandtl number for ε
τ	shear stress
τ_ω	wall shear stress
τ^+	dimensionless stress, τ/τ_ω
Φ	viscous dissipation
Ω	disk angular velocity.

Due to enclosure asymmetries and the presence of objects between the disks, the flow fields in practical disk storage systems are highly complex and unsteady. While it is important to render such flows amenable to numerical prediction, it is appropriate to first study unobstructed, axisymmetric configurations. As will be shown, such configurations result in very interesting phenomena in their own right and constitute a major challenge both from the numerical calculation and turbulence modelling points of view.

1.2. *Earlier work*

Because this is a computational study, the literature pertaining to numerical calculations utilizing phenomenological models of turbulence is of special interest. This is discussed below, following a summary of related experimental investigations.

1.2.1. *Experimental studies.* Reviews of free-spinning and corotating disk flows have been given in refs. [1, 2]. Here we present information pertinent to centrally clamped, unobstructed, coaxial disks corotating in an axisymmetric enclosure.

The visualization experiments of refs. [2–5] provide qualitative insight concerning the effect of configuration geometry on the flows that arise between and about two or more corotating disks. In particular, these studies reveal circumferentially periodic, radially directed inflows and outflows associated with axially-aligned vortical structures that are induced by shearing of the flow at the shroud. The visualization experiments of refs. [2, 3] are for disk configurations that are very similar to the one studied here. They show clearly that at a fixed rotational speed the axial vortices form an approximately regular polygon and that they vary discretely in number from 6 (at low rotational speeds) to 2 (at high rotational speeds).

This variation has been determined quantitatively in ref. [6] from time-resolved velocity measurements obtained with a laser-Doppler velocimeter. At high rotational speeds, the circumferential component of motion of the axial vortices has been stated in ref. [3] to lag behind the local disk speed by about 20%. The axial vortices appear to be the result of a circumferentially periodic Kelvin–Helmholtz instability [5]. In the disk pack experiment of ref. [4] the vortices were removed by blowing radially outwards in the space between each pair of disks.

Horizontal roll vortices have also been observed in enclosed corotating disk flows [3]. They have the form of equi-angular spirals and are embedded in the disk boundary layer which is of the order of $\delta = (\nu/\Omega)^{1/2}$. In ref. [3] the roll vortices were distributed over the whole surface of a disk, as of a disk Reynolds number $Re_r = 8.1 \times 10^5$ approximately, where $Re_r = \Omega R_2^2/\nu$, R_2 being the radius of the disk. The spirals appear to be manifestations of the Ekman layer instability which has been investigated in the free-spinning disk studies of refs. [7, 8–11].

The observations in ref. [3] showed that transition to turbulence in the space between corotating disks first occurred at the disk periphery, and that the turbulence advanced radially inwards with increasing rotational speed. The time-resolved velocity measurements of ref. [6] have revealed that transition to turbulent flow is preceded by a transition from steady laminar flow to sinusoidal unsteady laminar flow. With reference to Fig. 1, in the test section of ref. [6]: $H = 0.95$ cm, $a/H = 0.28$, $(R_2+a-R_1)/H = 5.40$, $R_2/R_1 = 1.85$, and $7.6 \times 10^3 < Re < 3.1 \times 10^4$, where $Re = \Omega R_2 H/\nu$. The sinusoidal unsteadiness first appeared at about $Re = 410$, corresponding to 62 ± 2 rpm, and turbulence was first detected in the vicinity of the shroud for $Re > 2150$, corresponding to 325 rpm. The measurements in ref. [6] were made in the space between the center pair of four corotating disks. With the same apparatus (same dimensions) and instrumentation, ref. [12] obtained time-averaged mean and r.m.s. values of the circumferential velocity component for the case when the outer pair of disks is fixed and the center pair corotate. The latter data was used to evaluate the numerical model(s) studied here.

Velocity measurements in the space between a pair of rotating coaxial disks of very large aspect ratio, $(R_2-R_1)/H$, were made in ref. [13], primarily in the laminar flow regime, and in ref. [14] in the turbulent regime. Turbulent isothermal flow in a rotating cylindrical cavity has been investigated in refs. [15, 16], while heat transfer measurements in the same configuration have been made in refs. [17, 18]. In ref. [18] the authors specifically investigated the effects of an imposed radial outflow between disks. Together with the measurements of ref. [12], the data in refs. [14, 18] have served to check the extension of the laminar flow numerical procedure of ref. [19] to turbulent flow, the subject of this work.

1.2.2. *Theoretical studies.* Since the seminal paper [20], there have been a number of proposals for turbulence closure schemes that avoid the use of wall functions as empirical 'patches' in wall-bounded flows. A systematic evaluation of eight of these models was conducted in ref. [21]. The use of wall functions requires high Reynolds numbers (so that viscous effects are negligible) and a knowledge of what wall functions to actually apply. In the complex corotating disk flows of interest here, neither condition can be satisfied and the wall function approach must be abandoned. The low Reynolds number models reviewed in ref. [21] incorporate wall damping effects and/or the direct effects of molecular viscosity in the modelled equations for the kinetic energy of turbulence, k, and its rate of dissipation, ε. Thus, these effects are already accounted for when the turbulent viscosity is evaluated from k and ε. Low Reynolds number models are computationally intensive, requiring dense grids in near wall regions. In addition, this modelling approach still needs improvement if it is to be used with confidence to predict near wall flows. Of the models evaluated by ref. [21], those due to refs. [22, 23] are of special interest here. Specifically, the model in ref. [22] has been used successfully to predict the flow over a free-spinning disk; and with the Richardson number modifications for curvature described in ref. [24], to also predict the flows around rotating cones and cylinders.

A less rigorous but much simpler way to account for wall damping effects is to use a modified van Driest relation [25] to specify the mixing length in the near wall region. This approach was discussed in ref. [20] where it was pointed out that entirely satisfactory prescriptions of the mixing length are rarely possible. Notwithstanding, a modified van Driest relation was employed in ref. [26] to prescribe the mixing length in an extended version of Prandtl's mixing length hypothesis that accounted for the effects of swirl on the turbulent viscosity. The mixing length derived from the van Driest relation was further modified, by using a Richardson number factor to account for the direct effects of swirl. The model derived in ref. [26] was successfully used to predict the flows around rotating disks, cones and cylinders. The discrepancies observed between measurements and computations of the flows were attributed primarily to the assumption of an isotropic turbulent viscosity.

In a series of studies [27–29] the mixing length model of ref. [26] was used to predict fluid motion in several axisymmetric disk flow configurations. The cases considered include: one disk rotating between two fixed flat surfaces, with the enclosure wall stationary; two disks corotating, with the enclosure wall rotating with the disks. Conditions with and without radial throughflow were considered. Even though convergence difficulties were reported at high speeds, the results obtained showed better agreement with experiments and the integral solution than those obtained in an earlier study [30] using a standard, high Reynolds number, k–ε model.

Direct numerical simulations of unobstructed rotating disk flows with very large aspect ratio have been performed in refs. [31, 32] where their stability characteristics and transition to turbulence were investigated. Conservation equations were formulated in terms of the circumferential components of velocity and vorticity, and a streamfunction. These equations were solved on very fine grids subject to circumferentially- and radially-periodic boundary conditions. The results reveal unsteady cross-stream flows for various combinations of r/H and the inverse Ekman number, $E^{-1} = \Omega H^2/\nu$. Although interesting in its own right, the configuration considered in these studies represents a limiting case of the present work where shearing of the flow by the enclosure wall is dominant.

In concluding this section we note that the presence of axially-aligned vortices in the enclosed disk experiments, the number of which depends on the rotation speed, raises the question of possible multiple states for shrouded corotating disk flows. To our knowledge, this problem has not been investigated extensively and all we can presently say is that at high rotational speeds, for example, in excess of 1200 rpm in the experiment of ref. [6], the flow between shrouded corotating disks is highly unsteady over most of the space between the disks and the number of axial vortical structures tends to the limit of 2. In contrast, considerable theoretical work has been performed on the multiplicity of solutions of the cross-stream flow in unshrouded corotating disk configurations [33–39]. Except for ref. [36], in all cases $(R_2 - R_1)/H \gg 1$. The analyses show that the particular solutions found often depend on the initial flow conditions and that their multiplicity increases with increasing rotation speed. In this work, $(R_2 - R_1)/H = O(10)$, and the flow near the shroud is highly turbulent. Since the turbulent condition is the most stable state of motion, one anticipates a tendency to statistically stationary flow behavior with increasing rotational speed. This condition is implied in the numerical model discussed below.

1.3. *The present study*

The experimental work in shrouded corotating disk configurations reveals three-dimensional, circumferentially periodic, unsteady turbulent flows at the Reynolds numbers of practical interest. Because these flows are very difficult to compute in full detail, the question should be asked: to what extent will an axisymmetric (but three-dimensional), steady representation mimic reality? The objective of this study has been to quantify the validity of this approach and explain why such a simplified representation of unobstructed disk flows yields satisfactory results for the mean flow and heat transfer. The advantages of a simplified numerical formulation are obvious, if useful predictions can be made. Thus, a related objective has been to investigate via numerical computation the effects of rotation, relative dimensions and blowing on the flow between corotating disks in axisymmetric enclosures.

2. NUMERICAL CALCULATION PROCEDURE

This section summarizes the conservation equations and boundary conditions computed numerically. The calculation algorithm is essentially that of ref. [40], extended and tested in ref. [19] for laminar disk flows and, as explained here, for turbulent flows. Three turbulence models were explored, of which two were low-Reynolds number formulations. However, the majority of the results presented in Section 3 are computed using a variant of the van Driest mixing length relation within the context of a Prandtl mixing length formulation.

2.1. *Conservation equations and boundary conditions*

The equations presented here assume statistically stationary, axisymmetric, constant property flow. They are written in final modelled form, in cylindrical coordinates, using the notation in Fig. 1. Reynolds decomposition and time averaging were applied to obtain the turbulent fluxes of momentum and heat. The flux of momentum was modelled using a generalization of the Boussinesq assumption, which uses an isotropic turbulent viscosity to relate the turbulent stress to the rate of strain. Similarly, the turbulent heat fluxes were modelled in terms of an isotropic eddy diffusivity multiplied by the appropriate mean temperature gradient.

2.1.1. *Continuity, momentum and energy.*

Continuity

$$\frac{1}{r}\frac{\partial}{\partial r}(rU) + \frac{\partial W}{\partial z} = 0 \tag{1}$$

r-momentum

$$U\frac{\partial U}{\partial r} + W\frac{\partial U}{\partial z} = -\frac{1}{\rho}\frac{\partial P}{\partial r} + \frac{1}{r}\frac{\partial}{\partial r}\left[r\left(2\nu_e\frac{\partial U}{\partial r}\right)\right] + \frac{\partial}{\partial z}\left[\nu_e\left(\frac{\partial U}{\partial z} + \frac{\partial W}{\partial r}\right)\right] - 2\nu_e\frac{U}{r^2} + \frac{V^2}{r} \tag{2}$$

z-momentum

$$U\frac{\partial W}{\partial r} + W\frac{\partial W}{\partial z} = -\frac{1}{\rho}\frac{\partial P}{\partial z} + \frac{1}{r}\frac{\partial}{\partial r}\left[r\nu_e\left(\frac{\partial W}{\partial r} + \frac{\partial U}{\partial z}\right)\right] + \frac{\partial}{\partial z}\left[2\nu_e\frac{\partial W}{\partial z}\right] \tag{3}$$

θ-momentum

$$U\frac{\partial V}{\partial r} + W\frac{\partial V}{\partial z} = \frac{1}{r^2}\frac{\partial}{\partial r}\left[r^3\nu_e\frac{\partial}{\partial r}\left(\frac{V}{r}\right)\right] + \frac{\partial}{\partial z}\left[\nu_e\frac{\partial V}{\partial z}\right] - \frac{UV}{r} \tag{4}$$

energy

$$U\frac{\partial T}{\partial r}+W\frac{\partial T}{\partial z}=\frac{1}{r}\frac{\partial}{\partial r}\left(r\alpha_e\frac{\partial T}{\partial r}\right)+\frac{\partial}{\partial z}\left(\alpha_e\frac{\partial T}{\partial z}\right)+\Phi \quad (5)$$

where the pressure term, P, includes the $2/3\rho k$ term associated with the normal components of the turbulent stress tensor and the quantity $\Phi=\nu_e P_k/C_p$ is the total conversion of mechanical energy into heat due to direct (viscous) and indirect (turbulent) dissipation.

2.1.2. *The turbulence models.* In the mean transport equations, the effective kinematic viscosity is given by $\nu_e=\nu_t+\nu$ where the turbulent component, $\nu_t=C_\mu f_\mu k^2/\varepsilon$. In this expression, C_μ is a constant and f_μ an empirical function that accounts directly for wall-damping of the turbulent diffusion process. The turbulent length and velocity scales in ν_t are found in terms of the turbulent kinetic energy, k, and its total rate of dissipation, ε. Therefore, additional conservation equations are required for these two quantities. In modelled form, these equations are:

k-equation

$$U\frac{\partial k}{\partial r}+W\frac{\partial k}{\partial z}=\frac{1}{r}\frac{\partial}{\partial r}\left(r\lambda_k\frac{\partial k}{\partial r}\right)+\frac{\partial}{\partial z}\left(\lambda_k\frac{\partial k}{\partial z}\right)+G-\varepsilon-D \quad (6)$$

ε-equation

$$U\frac{\partial \varepsilon}{\partial r}+W\frac{\partial \varepsilon}{\partial z}=\frac{1}{r}\frac{\partial}{\partial r}\left(r\lambda_\varepsilon\frac{\partial \varepsilon}{\partial r}\right)+\frac{\partial}{\partial z}\left(\lambda_\varepsilon\frac{\partial \varepsilon}{\partial z}\right)+C_1 f_1\frac{\varepsilon}{k}G-C_2 f_2\frac{\varepsilon^2}{k}+E \quad (7)$$

where the effective turbulent diffusivities for k, ε and T are given by: $\lambda_k=\nu_t/\sigma_k+\nu$, $\lambda_\varepsilon=\nu_t/\sigma_\varepsilon+\nu$ and $\alpha_e=\nu_t/\sigma_T+\alpha$ with σ_k, σ_ε and σ_T representing the pertinent turbulent Prandtl numbers.

The quantity $G=\nu_t P_k$ is the stress generation term in the k equation where

$$P_k=2\left[\left(\frac{\partial U}{\partial r}\right)^2+\left(\frac{\partial W}{\partial z}\right)^2+\left(\frac{U}{r}\right)^2\right]+\left[\frac{\partial W}{\partial r}+\frac{\partial U}{\partial z}\right]^2+\left[r\frac{\partial}{\partial r}\left(\frac{V}{r}\right)\right]^2+\left[\frac{\partial V}{\partial z}\right]^2. \quad (8)$$

The quantities represented by D, E, f_μ, f_1 and f_2 in the above equations depend on the turbulence model. Table 1 shows their respective functional form for the three cases explored and includes numerical values for the remaining model constants.

In the present formulation, the van Driest model reduces to a standard high-Reynolds number k–ε model in the core flow. In the vicinity of a wall, the turbulent viscosity is found using a generalization of Prandtl's mixing length hypothesis, namely

$$\nu_t=l_0^2 P_k^{1/2} \quad (9)$$

Table 1. Summary of turbulence model functions and constants for models of Launder and Sharma [22] (L. S), Lam and Bremhorst [23] (L. B) and van Driest [25] (VD)

Model	f_μ	f_1	f_2	D	E
LS	$\exp[-3.4/(1+R_t/50)]$	1.0	$1.0-0.3\exp(-R_t^2)$	$2\nu[(\partial k^{1/2}/\partial z)^2+(\partial k^{1/2}/\partial r)^2]$	$2\nu\nu_t[(\partial^2 U/\partial z^2)^2+(\partial^2 V/\partial z^2)^2+(\partial^2 W/\partial r^2)^2+(\partial^2 V/\partial r^2)^2]$
LB	$[1-\exp(-A_\mu R_k)]^2[1+A_1/R_t]$	$1+(0.05/f_\mu)^3$	$1-\exp(-R_t^2)$	0	0
VD	1.0	1.0	1.0	0	0
MVD	Like VD model except that wall shear (equation (11)) and curvature (equations (12) and (13)) modifications included				
MVD*	Like MVD except that l_0^2 in equations (9) and (10) replaced by equation (17)				

In the above: $A_\mu=0.0165$, $A_1=20.5$, $R_t=k^2/\nu\varepsilon$ and $R_k=k^{1/2}y/\nu$.
Additionally: $C_\mu=0.09$, $C_1=1.44$, $C_2=1.92$, $\sigma_T=0.9$.

where the mixing length, l_0, is given by the van Driest relation [25]. The mathematical interface between these two submodels is determined by: (a) requiring that the turbulent viscosity vary continuously from the wall region to the core of the flow; and (b) assuming that the turbulence is in equilibrium (production equals dissipation) in the region overlap. With these conditions one finds at the interface

$$k = \frac{l_0^2 P_k}{C_\mu^{1/2}} \quad \text{and} \quad \varepsilon = l_0^2 P_k^{3/2}. \tag{10}$$

These two equations provide the boundary conditions required to solve the k and ε equations in the core flow. The position of the matching wall–core interface is required to lie between $y^+ = 10$ and 50 for which preliminary numerical experimentation is necessary.

Two modifications were found to improve the present van Driest model calculations of mean velocity. The first was to adopt the proposal in refs. [26, 41] for modifying the mixing length, wherein the A^+ constant, an effective sublayer thickness, is divided by a power of the shear stress ratio, $\tau^+ = \tau/\tau_\omega$, to account for the variations in local stress near a wall. This amounts to specifying

$$l_0 = \kappa y \left[1 - \exp\left(-\frac{y^+}{A^+}(\tau^+)^{3/2}\right)\right]. \tag{11}$$

Although subsequent calculation showed it to be much less influential, the second modification represents an attempt to account for direct effects of curvature on the turbulence length scale. For this we specify, as in ref. [26], that $l_m = l_0(1 - \beta\, Ri)$, where Ri is an equivalent Richardson number for the curved flow, given by

$$Ri = \frac{2V\cos\alpha}{r^2}\frac{\partial rV}{\partial r}\left[\left(\frac{\partial W}{\partial r}\right)^2 + \left(r\frac{\partial V/r}{\partial r}\right)^2\right]^{-1}. \tag{12}$$

In this equation, $\beta = 5$ is an empirically determined constant and, following the convention in ref. [26], the value of $\cos\alpha$ is 0 in the region of flow adjacent to the disk surface and 1 in the region of flow adjacent to the shroud. The result is to increase l_m in the region of the flow adjacent to the concavely-curved shroud where the circumferential component of angular momentum decreases with increasing radius.

In keeping with the above curvature correction for the flow adjacent to the shroud, on the side of the matching interface near the shroud, where the k and ε equations are solved, we follow ref. [24] where $f_2 = 1 - C_c\, Ri_t$, with $C_c = 0.2$, an empirical constant, and where

$$Ri_t = \frac{k^2\cos\alpha}{\varepsilon^2}\frac{V}{r^2}\frac{\partial rV}{\partial r} \tag{13}$$

is now the appropriate form of the Richardson number, based on the local turbulence time scale.

2.1.3. *Boundary conditions.* The conservation equations were solved numerically subject to boundary conditions corresponding to four different corotating disk configurations. These are denoted Cases 1–4 and are listed below. In all cases the origin of the coordinates is located at the intersection of the axis of rotation and the geometrical symmetry plane between the two disks.

Case 1: corotating disks of zero thickness

$$U = 0, V = R_1\Omega, W = 0,$$

$$\text{at} \quad r = R_1 \quad \text{for} \quad 0 \leqslant z \leqslant \frac{H}{2}$$

$$U = 0, V = r\Omega, W = 0$$

$$\text{at} \quad z = \frac{H}{2} \quad \text{for} \quad R_1 \leqslant r \leqslant R_2$$

$$\frac{\partial U}{\partial z} = 0, \frac{\partial V}{\partial z} = 0, W = 0$$

$$\text{at} \quad z = \frac{H}{2} \quad \text{for} \quad R_2 \leqslant r \leqslant R_2 + a$$

$$U = 0, V = 0, W = 0$$

$$\text{at} \quad r = R_2 + a \quad \text{for} \quad 0 \leqslant z \leqslant \frac{H}{2}$$

$$\frac{\partial U}{\partial z} = 0, \frac{\partial V}{\partial z} = 0, W = 0$$

$$\text{at} \quad z = 0 \quad \text{for} \quad R_1 \leqslant r \leqslant R_2 + a.$$

Case 2: heated corotating disks of finite thickness

The boundary conditions for velocity are identical to Case 1 except that, for velocity

$$\frac{\partial U}{\partial z} = 0, \frac{\partial V}{\partial z} = 0, W = 0$$

$$\text{at} \quad z = \frac{H}{2} + \frac{b}{2} \quad \text{for} \quad R_2 \leqslant r \leqslant R_2 + a$$

and, for temperature

$$T = T_H \quad \text{at} \quad r = R_1 \quad \text{for} \quad 0 \leqslant z \leqslant \frac{H}{2} + \frac{b}{2}$$

$$T = T_S \quad \text{at} \quad r = R_2 + a \quad \text{for} \quad 0 \leqslant z \leqslant \frac{H}{2} + \frac{b}{2}$$

$$\frac{\partial T}{\partial z} = 0 \quad \text{at} \quad z = 0 \quad \text{and} \quad z = \frac{H}{2} + \frac{b}{2}$$

$$\text{for} \quad R_1 \leqslant r \leqslant R_2 + a.$$

In this case, the energy equation reduces to the conduction equation in the solid disk.

Case 3: heated corotating disks of finite thickness with radial and axial blowing

$$U = U_H, V = R_1\Omega, W = 0, T = T_H$$

$$\text{at} \quad r = R_1 \quad \text{for} \quad -\frac{H}{2} \leqslant z \leqslant \frac{H}{2}$$

$$U = 0, V = r\Omega, W = 0, T = T_H$$

$$\text{at } z = \frac{H}{2} \text{ and } z = -\frac{H}{2} \text{ for } R_1 \leqslant r \leqslant R_2$$

$$\frac{\partial U}{\partial z} = 0, \frac{\partial V}{\partial z} = 0, \frac{\partial W}{\partial z} = 0, \frac{\partial T}{\partial z} = 0$$

$$\text{at } z = \frac{H}{2} \text{ for } R_2 \leqslant r \leqslant R_2 + a$$

$$U = 0, V = 0, W = 0, T = T_S$$

$$\text{at } r = R_2 + a \text{ for } -\frac{H}{2} - b \leqslant z \leqslant \frac{H}{2}$$

$$U = 0, V = R_2\Omega, W = 0, T = T_H$$

$$\text{at } r = R_2 \text{ for } -\frac{H}{2} - b \leqslant z \leqslant -\frac{H}{2}$$

$$U = U_G, V = V_G, W = W_G, T = T_G$$

$$\text{at } z = -\frac{H}{2} - b \text{ for } R_2 \leqslant r \leqslant R_2 + a.$$

The above third and sixth lines specify the boundary conditions in the gaps formed by the edges of the two disks and the shroud. To simulate the developing nature of the axially-directed flow we proceed as follows: (a) the gap values U_G, V_G and T_G are assumed to vary linearly with radius in the inlet gap region; (b) the corresponding values found at the top (exit plane) gap are used as the inlet conditions at the bottom (inlet plane) gap; (c) the magnitude of W_G at the bottom gap is fixed by the mass flow requirement and its velocity profile is taken as uniform.

Case 4: two corotating disks in an enclosure with fixed top and bottom walls

The boundary conditions for the previous three cases correspond to pairs of disks in an infinite disk stack. In the present case we consider the influence on the flow of fixed impermeable walls parallel to the disks. For this, two disks are placed a distance H apart, each disk being at a distance h from its respective fixed parallel wall. The hub, the fixed flat walls and the shroud compose the enclosure boundaries. The boundary conditions are

$$U = 0, V = R_1\Omega, W = 0$$

$$\text{at } r = R_1 \text{ for } 0 \leqslant z \leqslant \frac{H}{2} + b + h$$

$$U = 0, V = 0, W = 0$$

$$\text{at } z = \frac{H}{2} + b + h \text{ for } R_1 \leqslant r \leqslant R_2 + a$$

$$U = 0, V = 0, W = 0$$

$$\text{at } r = R_1 + a \text{ for } 0 \leqslant z \leqslant \frac{H}{2} + b + h$$

$$\frac{\partial U}{\partial z} = 0, \frac{\partial V}{\partial z} = 0, W = 0$$

$$\text{at } z = 0 \text{ for } R_1 \leqslant r \leqslant R_2 + a$$

$$U = 0, V = r\Omega, W = 0$$

$$\text{at } z = \frac{H}{2} \text{ and } z = \frac{H}{2} + b \text{ for } R_1 \leqslant r \leqslant R_2$$

$$U = 0, V = R_2\Omega, W = 0$$

$$\text{at } r = R_2 \text{ for } \frac{H}{2} \leqslant z \leqslant \frac{H}{2} + b.$$

The specification of boundary conditions for k and ε depends on the turbulence model used. The conditions used were

$$k_i = 0.03U_i^2 \quad \text{and} \quad \varepsilon_i = \frac{k_i^{3/2}}{0.005L} \tag{14}$$

at the inflow locations 'i' (hub and bottom gap), where $L = H$ at the hub boundary and $L = a$ at the inlet gap boundary.

At the outlet gap boundary (and the symmetry plane for non-blowing cases)

$$\frac{\partial k}{\partial z} = 0 \quad \text{and} \quad \frac{\partial \varepsilon}{\partial z} = 0. \tag{15}$$

At all solid walls

$$k = 0 \text{(L–S and L–B model)}$$

$$\varepsilon = 0 \text{(L–S model)}; \partial\varepsilon/\partial n = 0 \text{(L–B model)} \tag{16}$$

where n denotes distance normal to a wall. Wall boundary conditions for k and ε are not required in the VD model because the eddy diffusivity is obtained from a Prandtl–Taylor mixing length formulation.

To initialize the calculations for any model, we first specified $U = 0$, $V = \Omega r$, $W = 0$ and $P = 0$ throughout the flow and set near-wall and core values of k and ε conforming with the distributions established in developed straight channel flow. For all models, calculations showed that the results predicted for a given Reynolds number, using the numerical solution at a different Reynolds number to initialize the calculations, converged to the same numerical solution as that obtained by using the original initialization conditions first described.

2.2. *Finite difference approximations and solution procedure*

The calculation domain is subdivided into a variable density calculation grid, with control volumes (or cells) geometrically defined at the grid nodes for scalar quantities and between grid nodes for the velocity components. Finite difference approximations for the conservation equations are derived by volume integration over each cell, subject to specific rules concerning the evaluation of fluxes and sources terms [40, 42]. In this regard, the use of the QUICK scheme [43] for convective transport terms and of central differencing for the diffusion terms imparts global second-order accuracy to the difference equations on a uniform grid.

The set of algebraic finite difference equations is

solved recursively using the tridiagonal matrix algorithm. This is done as part of a solution procedure that is iterative in nature. In the sequence, initial values for all the dependent variables of the flow field are guessed or specified from a previous calculation. The cross-stream velocity components are then solved and a pressure correction is evaluated using the SIMPLE procedure described in ref. [42]. The pressure correction is used to update the pressure and cross-stream velocity components respectively and, from these quantities, the circumferential velocity component is obtained. At this point, the k and ε equations are solved to obtain ν_t and, if the van Driest model is employed, near wall values for ν_t are obtained from the Prandtl mixing length hypothesis. Finally, for non-isothermal flows, the energy equation is solved for temperature. This iteration sequence is repeated until the convergence criterion is satisfied. This is that the largest of the normalized residuals for mass, momentum or energy be less than 5×10^{-5}. The use of under-relaxation factors for the dependent variables helps stabilize the calculation sequence.

2.3. *Testing*

The numerical procedure has been carefully tested in the laminar flow regime; see ref. [19]. Additional turbulent flow verifications were conducted for this work, for which some of the rotating disk flow configurations investigated in refs. [14, 18] were computed. These tests serve four purposes: (1) they provide a comparative evaluation of the turbulence models investigated; (2) they establish the nature of the grids required to generate grid-independent results; (3) they confirm that rotation, heat transfer and blowing effects are accurately predicted; (4) they allow an evaluation of the assumption of steady axisymmetric flow, upon which we base the numerical calculation approach.

The first point is addressed in Figs. 2.1 and 2.2 which compare the various model predictions on a ($z = 26 \times r = 62$) grid with measurements of the average and r.m.s. circumferential velocity component for the configuration of ref. [12] rotating at 3600 rpm ($Re = 22\,860$). That configuration corresponds to Fig. 1, for which relative dimensions are given in Section 1.2.1. Because the disk thickness, b, was small ($b/H = 0.21$), boundary conditions corresponding to Case 1 were specified in these calculations. In the r.m.s. comparisons, the isotropic calculations of $(2/3k)^{1/2}$ have been multiplied by the factor 1.3 to account, approximately, for the anisotropy among the normal stresses and the larger levels of the circumferential r.m.s. component expected, especially near walls [44].

Of the models tested, the MVD model (see Table 1) yielded the best results for mean velocity at both 3600 and 1200 rpm (the latter data are not shown). All the models predicted a significant variation of V with respect to z near the shroud, which is not supported by the measurements. It would seem that the calculated cross-stream flow distorts the circumferential component of motion near the shroud more strongly than occurs in the experiment. A similar discrepancy appears in the r.m.s. results near the shroud which, around $z/H = 0$, shows calculated values of $\tilde{V}$ higher than those measured. The smoothness and flatness of both the V and $\tilde{V}$ profiles suggest a strong redistributive action of the turbulence on the flow near the shroud which none of the models correctly resolve.

In the VD and MVD calculations, $(2/3k)^{1/2}$ is obtained from a high Reynolds number turbulence model in the core of the flow. Near walls, the value of k is not required, but an approximate distribution for it can be computed using equation (10). This approach yields qualitatively correct results for the VD model but unrealistic results for the MVD calculations in part of the near wall flow. This is attributed to the τ^+ term in equation (11) which is proportional to ν_t and, since $\nu_t \propto l_0^2$, the exponent in equation (11) varies according to y^4. This causes a much faster decrease of l_0 in approaching a wall than is obtained using equation (11) as proposed by van Driest, *without* the $(\tau^+)^{3/2}$ term. In the region where l_0 starts to decrease quickly as a wall is approached, the velocity gradients normal to that wall are still small. Therefore, the P_k term in k is small and k decreases especially quickly. However, in continuing towards the wall a region is reached where the velocity gradients steepen quickly and, as a result, P_k also increases, but quadratically, thus offsetting the decrease in l_0 and raising the local value of k. This explains the jagged appearance of k near the wall for the MVD calculations.

As explained above, in the VD and MVD models, k and ε in the core are calculated using the boundary conditions stipulated by equations (10) at the sub-model matching interface. For the reasons just discussed, the interface boundary values are unrealistically small. In an attempt to retain the accuracy of the MVD model for predicting V with the more realistic results given for $\tilde{V}$ by the VD model, we replaced l_0^2 in equations (9) and (10) by the expression

$$(\kappa y)^2 \left[1 - \exp\left(-\frac{y^+}{A^+}\right)\right]\left[1 - \exp\left(-\frac{y^-}{A^-}(\tau^+)^{3/2}\right)\right]. \tag{17}$$

Results for this MVD* model are also shown in Figs. 2.1 and 2.2. They illustrate the level of compromise obtained between the predictions and measurements for V and $\tilde{V}$.

Fortunately, in a Prandtl mixing length formulation an incorrect prediction of k in the core flow does not directly affect the prediction of ν_t near a wall. The better predictions of V obtained with the MVD model suggest that this model better resolves the wall boundary layers of the rotating disk flow, and that the effects of turbulence in the core are of secondary importance. Accordingly, the MVD model was chosen for the rest of the numerical calculations performed.

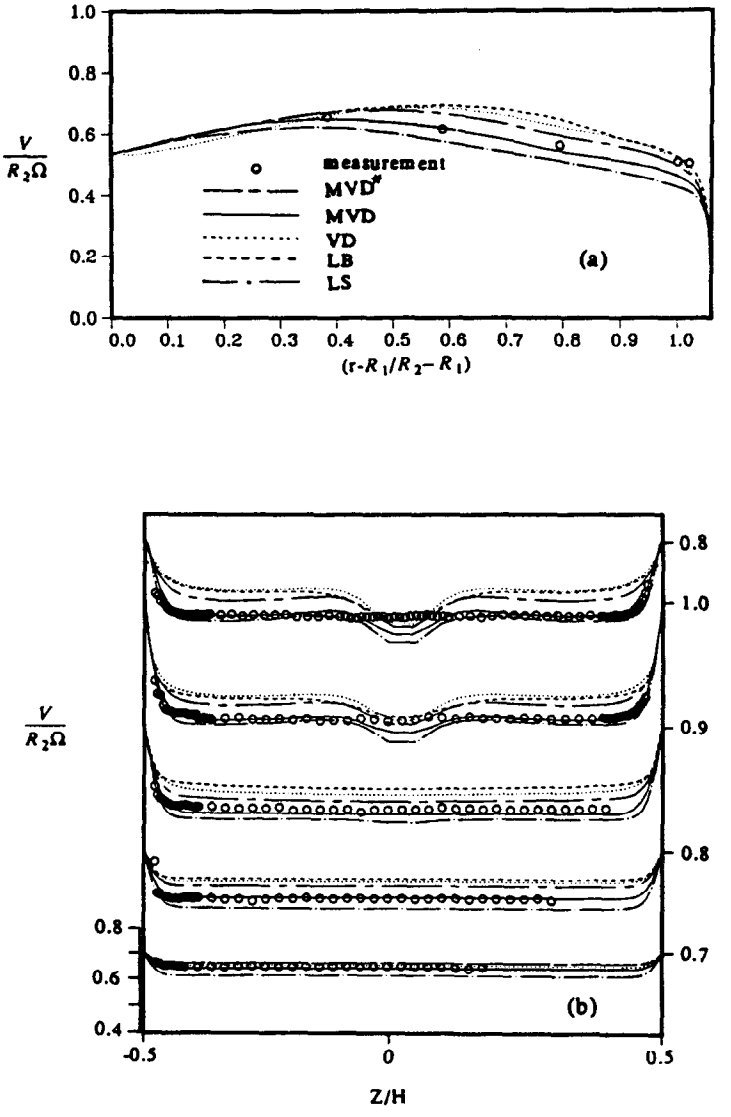

FIG. 2.1. Comparison between measurements and model predictions of the dimensionless average circumferential velocity (a) along the midplane ($z/H = 0$), (b) at $(r-R_1)/(R_2-R_1) = 0.38$, 0.59, 0.79, 1.00 and 1.02 (bottom to top) for 3600 rpm. Case 1 boundary conditions used. Ticks on the right-hand axis mark the location and value of the disk speed normalized by $R_2\Omega$ for the particular radial location.

It is noteworthy that the MVD model predicts coexisting turbulent and laminar regimes of motion without the artificial introduction of perturbations to induce transition to turbulent flow. This is due to the recirculating action of the cross-stream secondary motion which transports turbulent fluid near the shroud into the core of the flow, thus disseminating the fluctuating component of motion. In regions where the flow approaches the condition of solid body rotation, such as near the hub, the model correctly predicts that the turbulent viscosity, ν_t, tends to zero. Figure 3, showing contour plots of k and ν_t, illustrates this point.

The requirements for grid independence were analyzed by performing MVD model calculations of the above flow on three successively refined nonuniform grids. The predictions, available in ref. [45], revealed that a grid with ($z = 26 \times r = 62$) nodes gave mean velocity results that agreed to within 1% with those on a grid with ($z = 36 \times r = 74$) nodes. Typical corresponding changes in k and ε predicted on these two grids were 3 and 4%, respectively. On the basis of these findings, the intermediate ($z = 26 \times r = 62$) grid was chosen for the bulk of the numerical calculations and was distributed so as to contain not less than 10 nodes in the disk and shroud boundary layer regions, respectively. While the finer of the three grids would have yielded somewhat more accurate numeri-

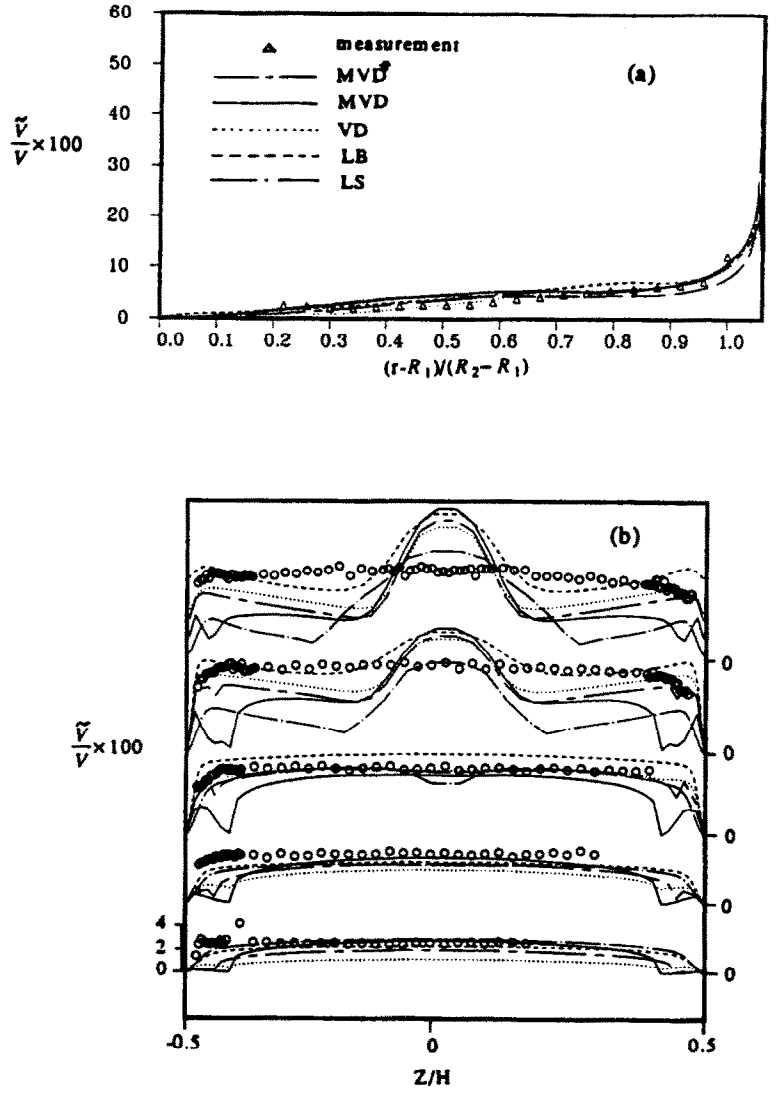

FIG. 2.2. Comparison between measurements and model predictions of the circumferential component of turbulence intensity (a) along the midplane ($z/H = 0$), (b) at $(r-R_1)/(R_2-R_1) = 0.38$, 0.59, 0.79, 1.00 and 1.02 (bottom to top) for 3600 rpm. Case 1 boundary conditions used.

cal calculations of k and ε, this was considered to be unnecessary given the insensitivity of the mean flow to the more refined calculations of k and ε.

The ability of the MVD numerical model to predict corotating disk flows with heat transfer and/or radial blowing was checked against the experimental data reported in refs. [14, 18]. Space limitations require that we summarize the tests reported in ref. [45]. In each case, two pairs of values of the radial blowing parameter, $C_r = Q_r/\nu R_2$, and Reynolds number, $Re = \Omega R_2 H/\nu$, were calculated where Q_r is the air volume flow rate between disks in the radial direction. For the isothermal flows in ref. [14], the pairs were ($C_r = 2507$, $Re = 4092$) and ($C_r = 3123$, $Re = 4077$), respectively. Axial profiles of the circumferential and radial velocity components plotted at $r/R_2 = 0.545$ for the first pair of values were in good agreement with the measurements. For the second pair, plotted at $r/R_2 = 0.773$, discrepancies of 10–20% were found for the radial velocity component only.

Similar calculations, including the radial distribution of the disk surface local Nusselt number, were performed for ($C_r = 1400$, $Re = 1.8 \times 10^4$) and ($C_r = 2800$, $Re = 4.4 \times 10^4$), two of several heat transfer cases with blowing investigated in ref. [18]. For the low blowing case agreement between measurements and calculations was good, but for the high blowing case the calculations overpredicted the mean Nusselt numbers by 10–20%. For both blowing and heating, the qualitative features of the velocity components and Nusselt numbers were correctly predicted. The combination of experimental uncertainty in the measurements ($\pm$5–10% for the mean

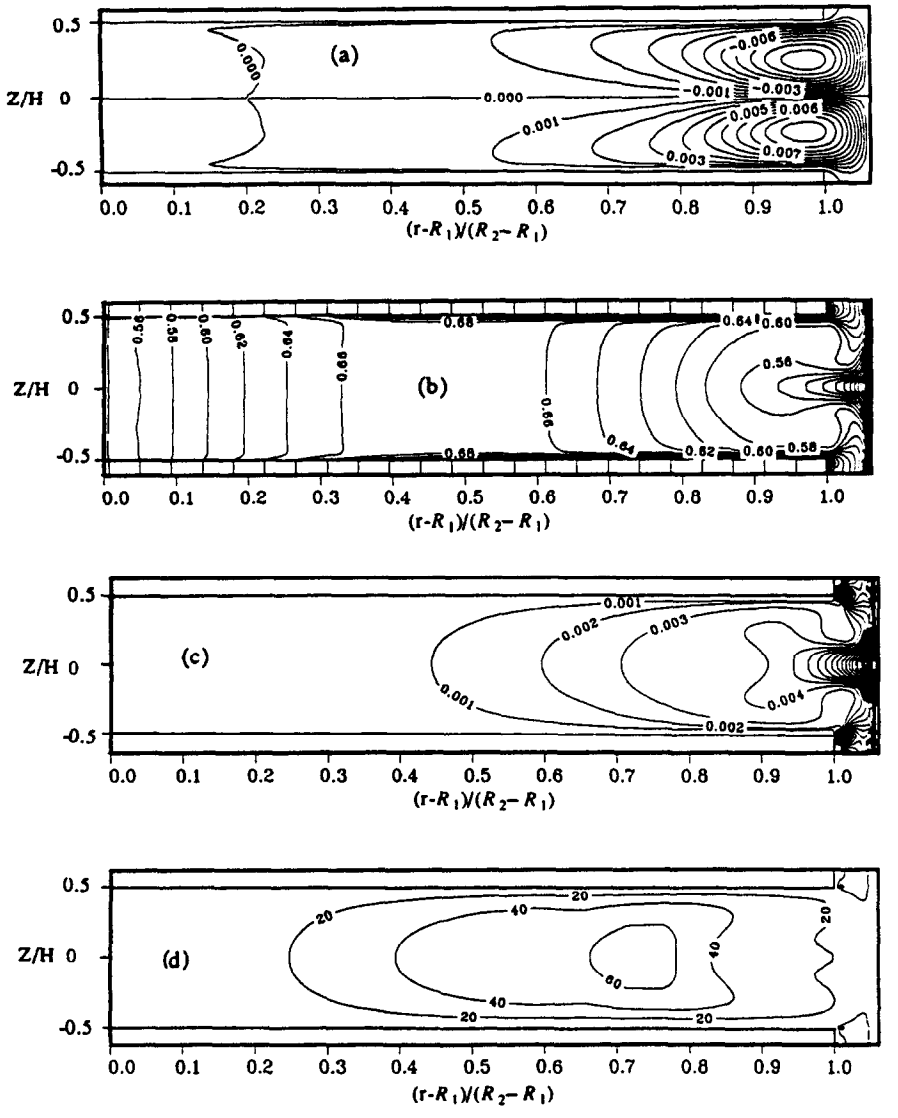

FIG. 3. MVD calculations for Case 2 boundary conditions at 3600 rpm. Plots show contours of (a) flow streamlines; (b) average circumferential velocity, $V/\Omega R_2$; (c) turbulent kinetic energy, k/V^2; (d) turbulent viscosity, ν_t/ν.

velocities and about $\pm$10–15% for the Nusselt numbers) and the limitations in the turbulence model combine to yield a predictive capability of the numerical procedure which is estimated to be within $\pm$15–25% in so far as predicting blowing and heat transfer effects.

In all the above, we have compared time-averaged measurements with numerical calculations based on the assumption of steady, statistically stationary, axisymmetric flow. The closeness of the agreement found with the circumferential mean velocity measurements of ref. [12] suggests that the significant mean flow unsteadiness observed experimentally (associated with circumferentially periodic axially-aligned vortical structures driven by shear instability) contributes sinusoidally to the instantaneous component of motion. A sinusoidal oscillation would not affect the mean of the instantaneous velocity signal but would alter its r.m.s. As explained below, this accounts for part of the discrepancy observed at low rpm between measurements of $\tilde{V}$ and its numerical estimate $(2/3k)^{1/2}$.

To resolve mean flow unsteadiness would require dispensing with the assumption of circumferential symmetry, which would significantly increase the calculation requirements. Fortunately, the tests performed show that the resolution of circumferential asymmetry and flow unsteadiness are not necessary to elucidate many quantitative and qualitative parameter dependencies of the present flow.

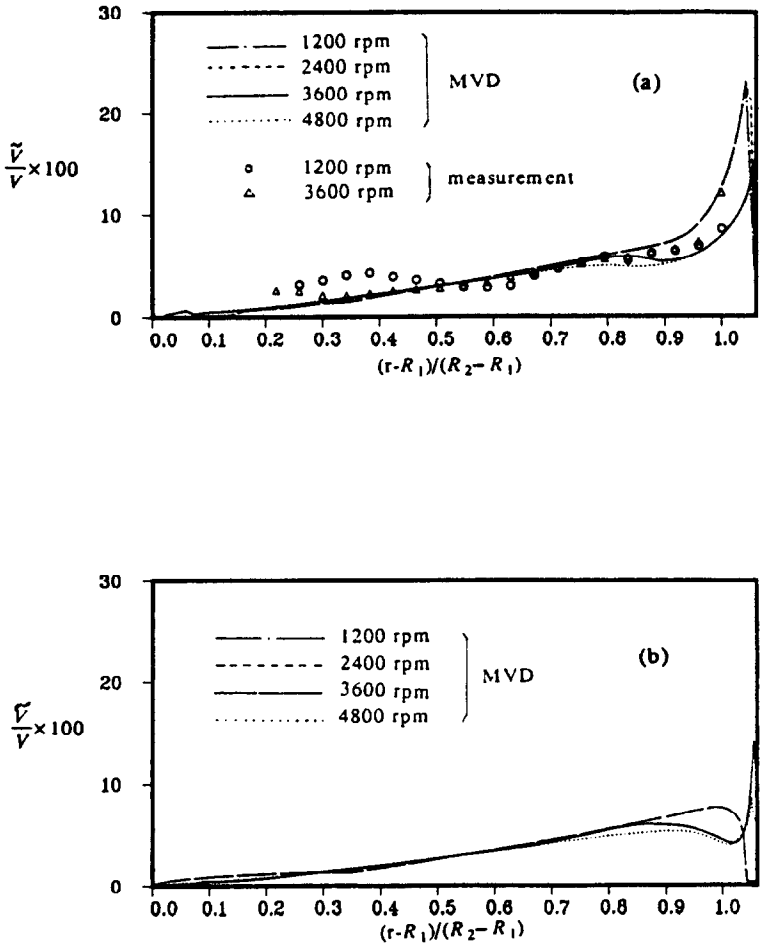

FIG. 4. MVD calculations of the circumferential component of turbulence intensity for Case 2 boundary conditions at 4 rpm along (a) the symmetry plane ($z/H = 0$), (b) the quarter plane ($z/H = 0.25$).

Calculations for Case 1-type boundary conditions on a ($z = 26 \times r = 62$) grid typically required about 2000 iterations to attain the convergence criterion, amounting to 360 CPU s on the Berkeley Campus Cray X-MP computer.

3. NEW RESULTS AND DISCUSSION

The MVD numerical model was used to study the effects of disk rotation, geometry and blowing conditions on the flow corresponding to the configuration of Fig. 1. This configuration is identical to that explored experimentally in ref. [12], the time-averaged data of which were used above for validation purposes. We summarize here the main findings of the numerical exploration, noting that more extensive and detailed results are available in ref. [45].

3.1. *Influence of rotation*

Calculations were performed for 1200, 2400, 3600 and 4800 rpm, corresponding to values of the Reynolds number, Re, equal to 7620, 15240, 22860 and 30480, respectively. Figure 3 shows some of the results for 3600 rpm. The streamlines reveal a symmetrical pair of eddies that are due to the pressure-driven cross-stream secondary motion. The circumferential velocity contours show that the flow near the hub approaches solid body rotation, while that nearer the shroud is strongly sheared and, as shown by the turbulent kinetic energy contours, is associated with the largest fluctuations in the flow. The cross-stream secondary motion convects low speed highly turbulent fluid from the shroud towards the hub along the symmetry plane of the flow. This results in a penetration of the turbulence to $(r-R_1)/(R_2-R_1) = 0.5$ approximately, which coincides with the position of maximum circumferential velocity.

Comparisons with time averaged measurements corresponding to this flow were presented and discussed above. The experimental results show, and the calculations confirm, that the characteristics of the mean flow tend to an asymptotic limiting state with increasing Reynolds number. In this regard, computations of the dimensionless mean velocity com-

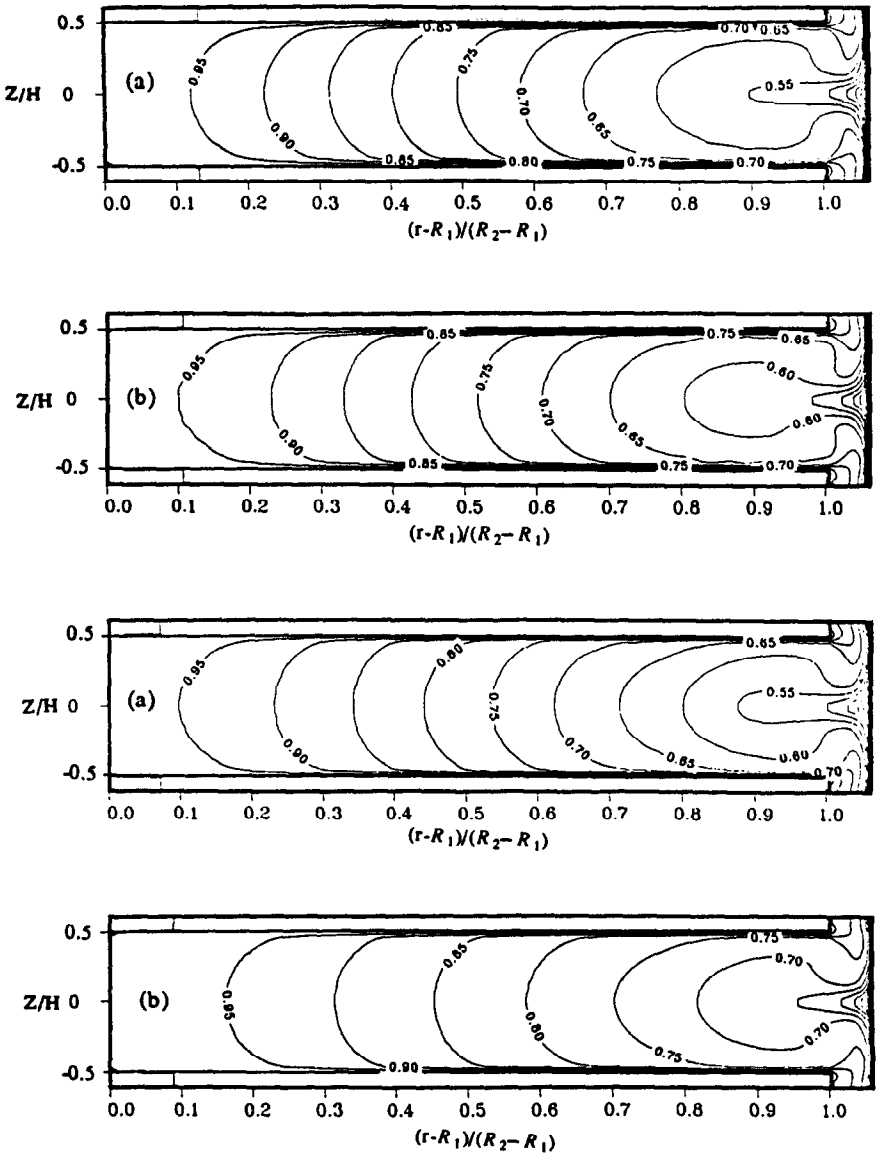

FIG. 5. MVD calculations of $(T-T_S)/(T_H-T_S)$ for Case 2 boundary conditions at 3600 rpm (top) and 4800 rpm (bottom) without (a) and with (b) dissipation included.

ponents at the four rotational speeds were essentially identical. However, the computed values of k and ε (and of temperature when dissipation is important) were dependent on rpm. Plots showing this dependence for k and T are given in Figs. 4 and 5, respectively. At 1200 rpm there is a significant discrepancy between the measured and calculated k-profiles along $z/H = 0$ between $(r-R_1)/(R_2-R_1) = 0.2$ and 0.45. This is attributed to the circumferentially-distributed axially-aligned vortical structures discussed earlier, which contribute to the r.m.s. of the velocity component without significantly affecting its average value.

The temperature calculations in Fig. 5 were performed with $T_H - T_S = 10°C$, with and without the inclusion of dissipation. All other calculations in this work were performed with dissipation included. The isotherms are strongly distorted in the sense of the cross-stream secondary flow, illustrating the importance of convective heat transport for the distribution of thermal energy between the disks. The relatively high conductivity of the disks, modelled as aluminum, explains that their temperature is essentially that of the hub, T_H.

A shroud wall Nusselt number was defined by

$$Nu = \frac{1}{t}\int_0^t \frac{q_w R_2}{K(T_H - T_S)}\,dz \tag{18}$$

where $t = H/2 + b/2$. This is plotted in Fig. 6, with and without the inclusion of dissipation, as a function of

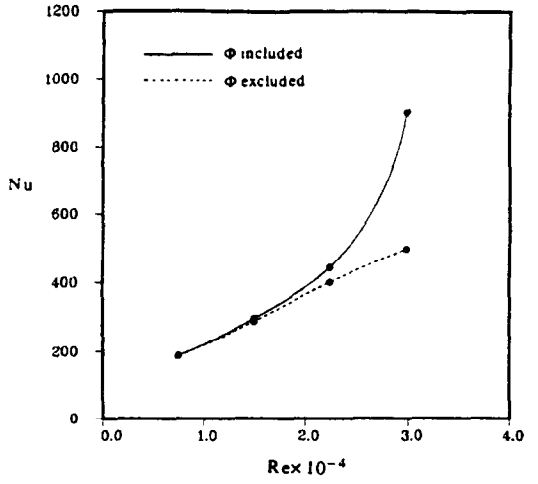

FIG. 6. MVD calculations of shroud wall Nusselt number as a function of Reynolds number with and without dissipation included for Case 2 boundary conditions.

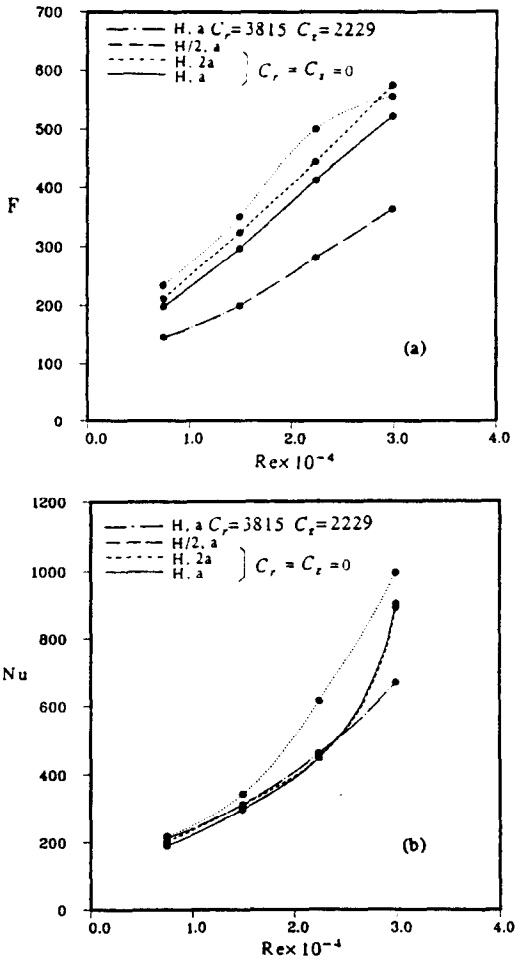

FIG. 7. Dimensionless shear stress (a) and Nusselt number (b) for different geometrical dimensions with (Case 3 boundary conditions) and without (Case 2 boundary conditions) blowing as a function of Reynolds number.

Reynolds number. The profiles suggest that dissipation becomes significant between 2400 and 3600 rpm. At 4800 rpm the ratio of the disk tip speed to the speed of sound is $\Omega R_2/c = 0.15$, justifying the neglect of compressibility effects in the flow.

3.2. *Influence of geometry*

Two values of the disk separation (H and $H/2$) and of the gap width (a and $2a$) were investigated. Detailed plots of the corresponding flow fields are given in ref. [45]. Figures 7(a) and (b) show the dependence of the dimensionless shroud wall shear, F, and Nusselt number, Nu, on H and a as a function of the Reynolds number. The dimensionless wall shear was defined by

$$F = \frac{1}{t}\int_0^t \frac{\tau_{\omega}}{\mu\Omega}\,\mathrm{d}z. \tag{19}$$

For a fixed rotational speed, reducing H to $H/2$ significantly increased the viscous effects relative to the standard (H, a) case. This was noticeable in the increased values of shear, dissipation and temperature near the shroud, and in the enlargement of the solid body rotation region around the hub.

Increasing a to $2a$ constrained the bulk of the cross-stream secondary motion to a smaller flow region close to the shroud. In this region, even though the gap spacing was doubled, the shear increased slightly relative to the standard (H, a) case, but changes in temperature and in the Nusselt number were very small. A detailed inspection of the streamline plots in ref. [45] shows that increasing the gap width allows the cross-stream flow to penetrate the disk edge-gap region more completely, thus steepening the V-profile normal to the shroud and increasing the value of the shear slightly.

The bulk of this study has focused on the flow between a pair of disks in an infinite stack. Depending on whether the disks are heated and or blowing is applied, boundary conditions corresponding to Cases 1–3 above apply. To understand the influence on the flow due to the presence of non-rotating walls parallel to the disks, the boundary conditions corresponding to Case 4 were investigated. Figure 8 shows streamline and circumferential velocity contours for a flow at 3600 rpm. The calculations were performed on a grid that had ($z = 26 \times r = 62$) nodes between the symmetry plane and a rotating disk and ($z = 31 \times r = 62$) nodes between a disk and its corresponding fixed wall. Additional cases are plotted in ref. [45]. Between the pair of rotating disks the flow is very similar to that shown in Fig. 3, for a pair of disks in an infinite stack. A single cross-stream eddy appears between each rotating disk and its corresponding fixed parallel wall. This eddy penetrates all the way to the hub where the solid body rotation flow condition cannot be maintained. While the single eddy between a fixed wall and a rotating disk recirculates faster than either one of the symmetrical eddies between the pair of corotating

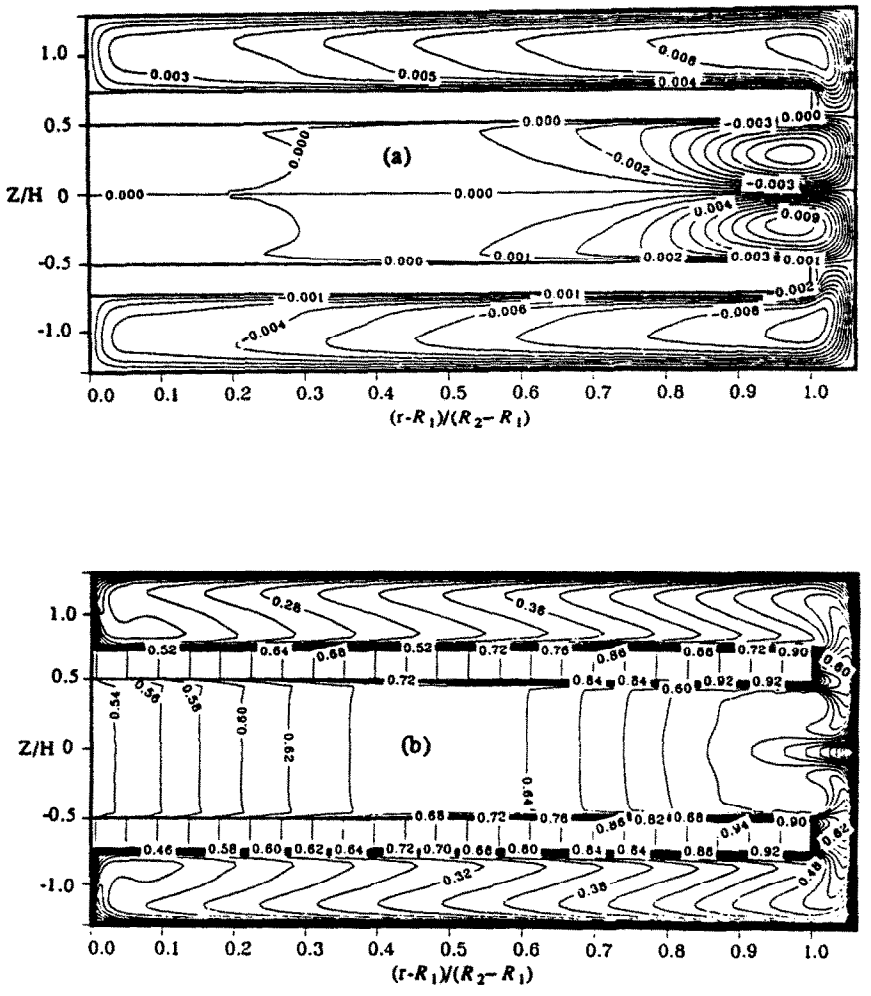

FIG. 8. Streamlines (a) and circumferential velocity (b) contours at 3600 rpm calculated for Case 4 boundary conditions.

disks, the average circumferential velocity at any radial location in the first space is lower than in the second. The result is for a pressure gradient, acting from the first space into the second, to deflect the motion in the gap region. The consequence of this is a lack of symmetry of the cross-stream flow with respect to horizontal planes passing through $z = H/2+b/2$ and $-H/2-b/2$, respectively. (Notwithstanding, the reader should recall from earlier discussion that the assumption of symmetry yielded calculations of the circumferential mean flow in very good agreement with the measurements of ref. [12] where the outer pair of disks was fixed and the inner pair corotated.) Further computations would reveal the minimum number of disks required to more closely attain the symmetry condition, but this was beyond the scope of the present work.

3.3. *Influence of blowing*

The dimensionless radial and axial blowing parameters are defined by $C_i = Q_i/(\nu R_2)$, where $i = r$ for the hub (radial blowing) and $i = z$ for the bottom inlet gap (axial blowing) and Q is the volume flow rate of air in the radial direction. Calculations were performed for various rpm with $C_z/C_r = 0.584$ and 5.84, respectively. The results for 2400 and 4800 rpm with $C_z/C_r = 0.584$ are shown in Figs. 9 and 10. At the lower rotational speed the radial blowing condition dictates the streamline flow pattern in the space between the disks; the influence of the axial component of motion being reduced to a region adjacent to the shroud no larger than the gap. At the high rotational speed, the Ekman boundary layers on the disks are more clearly defined. In this case a single counter-clockwise rotating cross-stream eddy appears near the shroud. The corresponding plots for the circumferential velocity component and temperature should be compared with the non-blowing case at 3600 rpm shown in Fig. 3. It is clear that the imposition of radial blowing significantly reduces the circumferential velocity component everywhere in the space between the disks. For the conditions shown,

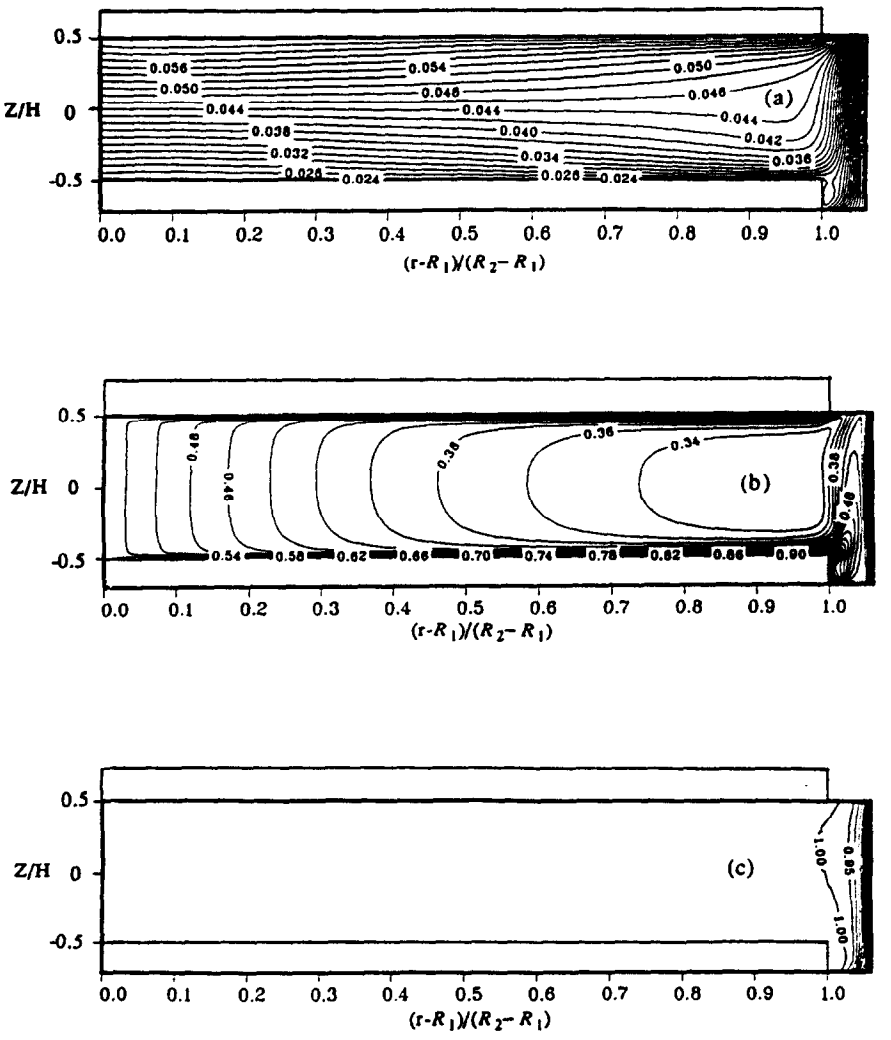

FIG. 9. MVD calculations for Case 3 boundary conditions with radial ($C_r = 3815$) and axial ($C_z = 2229$) blowing at 2400 rpm; plots show contours of (a) flow streamlines; (b) average circumferential velocity, $V/\Omega R_2$; and (c) temperature $(T-T_S)$ (T_H-T_S).

radial blowing eliminates the cross-stream flow and homogenizes the temperature distribution between the disks. For fixed rpm, increasing the ratio C_z/C_r from 0.584 to 5.84 did not significantly alter the qualitative aspects of the flows shown in Figs. 9 and 10.

Figure 7 showed the effect of combined radial and axial blowing on the shear and heat transfer at the shroud as a function of rotational speed. Similar results, computed for laminar flow in ref. [19], show that pure radial blowing significantly increases shear and heat transfer relative to no blowing. This is due to the steeper gradients of circumferential velocity and temperature which radial blowing induces at the shroud. By contrast, present calculations show that blowing air axially through the gap protects the shroud from the gradient-steepening influences of radial blowing. This is a useful finding, for it allows the combination of radial blowing, to remove flow structures and heat from the regions between disks, with axial blowing, to avoid their accumulation on the shroud.

4. CONCLUSIONS

This numerical study has shown that the mean velocity and heat transfer characteristics in most of the space between a pair of disks corotating in an axisymmetric enclosure can be accurately predicted using a Prandtl mixing length formulation for near wall flow regions with a modified van Driest relation for the mixing length. More accurate predictions of the turbulent kinetic energy near the rotating disks and shroud are obtained using an unmodified van Driest relation in the mixing length approach or, alternatively, with a low-Reynolds number turbulence model formulation, but this is at the expense of less

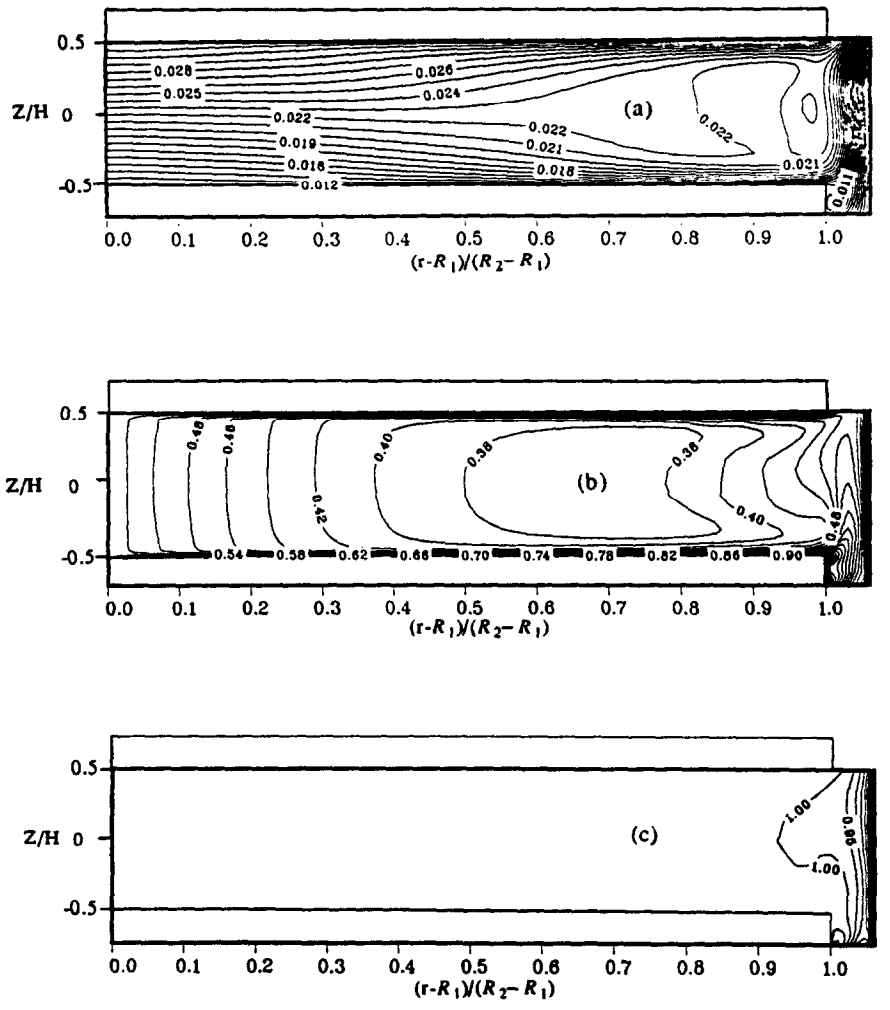

FIG. 10. MVD calculations for Case 3 boundary conditions with radial ($C_r = 3815$) and axial ($C_z = 2229$) blowing at 4800 rpm; plots show contours of (a) flow streamlines; (b) average circumferential velocity, $V/\Omega R_2$; and (c) temperature $(T-T_S)/(T_H-T_S)$.

accurate mean velocity results. All the models explored in this study overpredict the intensity of the cross-stream secondary motion near the shroud and its effect on the distribution of the turbulent kinetic energy. The result is a larger penetration of flow from the shroud region into the core than actually takes place. Presumably, therefore, the distributions of other convected scalar quantities in this region, such as temperature, are also subject to a similar erroneous distribution.

The numerical procedure is based on the assumption of steady, circumferentially symmetric flow. However, time-resolved measurements reveal an unsteady, circumferentially periodic motion. Notwithstanding, the predictions show very good agreement with time averaged measurements of mean velocity and heat transfer in most of the flow. Discrepancies that arise between measurements and calculations of the velocity r.m.s. in the core of the flow are attributed to non-turbulent, large-scale, circumferentially periodic vortical structures that arise from intense shearing of fluid at the curved enclosure wall and which are not resolved numerically. The magnitude of this discrepancy appears to decrease with increasing disk rotational speed, a condition which favors an asymptotic limit state for the flow at high Reynolds number. From these findings we tentatively conclude that the non-turbulent oscillatory component of motion must be close to sinusoidal in nature and, while it affects the measured r.m.s., it has little or no influence on the time-averaged velocity.

The numerical procedure was used to explore the effects of rotation, geometry and blowing on the flow and heat transfer in the space between the disks. The results show that viscous heating of the air is significant as of 2400 rpm for the configuration(s) of interest. Decreasing the spacing between disks leads to increased shear and heat transfer at the shroud

wall. Increasing the gap width between the rotating disks and the shroud wall does not significantly affect the heat transfer but, surprisingly, slightly increases the shear on the shroud. Whether the surfaces parallel to the rotating disks are themselves rotating or stationary affects the flow (and hence the boundary conditions) in the disk–shroud gap. Through a combination of radial blowing between disks and axial blowing along the disk–shroud gap, flow structures and heat can be effectively removed from the region between disks while avoiding their accumulation (with the attendant increases in shear and heat transfer) on the shroud. This last point should be of special interest for the improved performance of disk storage devices in the computer industry.

Acknowledgements—The authors most gratefully acknowledge extensive discussions on the turbulence models, which were held with Professor B. E. Launder and Dr H. Iacovides at the University of Manchester, Institute of Science and Technology. Special thanks are due to Professor Launder for arranging for CJC to visit UMIST to refine the modelling approaches. This work and CJC's trip to UMIST were supported through a contract received from the IBM Almaden Research Center in San Jose, California. Part of the study was performed while JACH was a visiting research scholar there, during the summer of 1988. Many thanks go to Ms M. A. Peters and Ms S. Slavin for preparing this manuscript.

REFERENCES

1. J. A. C. Humphrey, Summary literature review on rotating disk flows, Report No. FM-86-2, Mechanical Engineering Department, The University of California at Berkeley (1986).
2. S. D. Abrahamson, D. J. Koga and J. K. Eaton, An experimental investigation of the flow between shrouded corotating disks, Report MD-50, Thermoscience Division, Department of Mechanical Engineering, Stanford University (1988).
3. E. Lennemann, Aerodynamic aspects of disk files, *IBM J. Res. Dev.* **18**(6), 480–488 (1974).
4. R. Kaneko, S. Oguchi and K. Hoshiya, Hydrodynamic characteristics in disk packs for magnetic storage, *Rev. Elect. Commun. Lab.* **25**(11–12), 1325–1336 (1977).
5. M. Rabaud and T. Couder, A shear-flow instability in a circular geometry, *J. Fluid Mech.* **136**, 291–319 (1983).
6. W. Usry, C. A. Schuler, J. A. C. Humphrey and R. Greif, Unsteady flow between corotating disks in an enclosure with an obstruction, *Proc. Fifth Int. Symp. on Application of Laser Techniques to Fluid Mechanics*, Lisbon, Portugal, July (1990).
7. E. C. Cobb and O. A. Saunders, Heat transfer from a rotating disk, *Proc. R. Soc., Ser. A, Math. Phys. Sci.* **236**, 343–351 (1956).
8. A. J. Faller, An experimental study of the instability of the laminar Ekman boundary layer, *J. Fluid Mech.* **15**, 560–576 (1963).
9. A. J. Faller and R. E. Kaylor, A numerical study of the instability of the laminar Ekman boundary layer, *J. Atmos. Sci.* **23**, 466–480 (1966).
10. A. J. Faller and R. E. Kaylor, Instability of the Ekman spiral with applications to the planetary boundary layers, *Physics Fluids* **10**, S212–S219 (1967).
11. P. R. Tatro and E. L. Mollo-Christensen, Experiments on Ekman layer stability, *J. Fluid Mech.* **28**, 531–543 (1967).
12. B. Weber, C. A. Schuler, J. A. C. Humphrey and R. Greif, Experimental investigation of the flow between corotating disks in an axisymmetric enclosure, *Proc. Third Int. Conf. on Laser Anemometry Advances and Applications*, University College of Swansea, Wales, 26–29 September (1989).
13. A. Z. Szeri, S. J. Schneider, F. Labbe and H. N. Kaufman, Flow between rotating disks (Part 1. Basic flow), *J. Fluid Mech.* **134**, 103–132 (1983).
14. E. Bakke, J. F. Kreider and F. Kreith, Turbulent source flow between parallel stationary and co-rotating disks, *J. Fluid Mech.* **58**, 209–231 (1973).
15. J. M. Owen and J. R. Pincombe, Velocity measurements inside a rotating cylindrical cavity with a radial outflow of fluid, *J. Fluid Mech.* **99**, 111–127 (1980).
16. J. M. Owen, J. R. Pincombe and R. H. Rogers, Source–sink flow inside a rotating cylindrical cavity, *J. Fluid Mech.* **155**, 233–265 (1985).
17. A. Northrop and J. M. Owen, Heat transfer measurements in rotating-disc systems, Part 1 : the free disc, *Int. J. Heat Fluid Flow* **9**(1), 19–26 (1988).
18. A. Northrop and J. M. Owen, Heat transfer measurements in rotating-disc systems, Part 2 : the rotating cavity with a radial outflow of cooling air, *Int. J. Heat Fluid Flow* **9**(1), 27–36 (1988).
19. C. J. Chang, C. A. Schuler, J. A. C. Humphrey and R. Greif, Flow and heat transfer in the space between two corotating disks in an axisymmetric enclosure, *J. Heat Transfer* **111**, 625–632 (1989).
20. W. P. Jones and B. E. Launder, The prediction of laminarization with a two-equation model of turbulence, *Int. J. Heat Mass Transfer* **15**, 301–314 (1972).
21. V. C. Patel, W. Rodi and G. Scheuerer, Turbulence models for near-wall and low Reynolds number flows: a review, *AIAA J.* **23**, 1308–1319 (1985).
22. B. E. Launder and B. I. Sharma, Application of the energy-dissipation model of turbulence to the calculation of flow near a spinning disc, *Lett. Heat Mass Transfer* **1**, 131–138 (1974).
23. C. K. G. Lam and K. A. Bremhorst, A modified form of the k–ε model for predicting wall turbulence, *J. Fluids Engng* **103**, 456–460 (1981).
24. B. E. Launder, C. H. Priddin and B. I. Sharma, The calculation of turbulent boundary layers on spinning and curved surfaces, *J. Fluids Engng* **99**, 231–239 (1977).
25. E. R. van Driest, On turbulent flow near a wall, *J. Aeronaut. Sci.* **23**, 1007–1036 (1956).
26. M. L. Koosinlin, B. L. Launder and B. I. Sharma, Prediction of momentum, heat and mass transfer in swirling, turbulent boundary layers, *J. Heat Transfer* **96**, 204–209 (1974).
27. J. W. Chew, Prediction of flow in a rotating cavity with radial outflow using a mixing length turbulence model, *Proc. Fourth Int. Conf. on Numerical Methods in Laminar and Turbulent Flow*, Swansea, Wales (1985).
28. J. W. Chew, Computation of flow and heat transfer in rotating disc systems, *Proc. 2nd ASME–JSME Thermal Engng Conf.*, Hawaii, pp. 361–367 (1987).
29. J. W. Chew and C. M. Vaughan, Numerical predictions for the flow induced by an enclosed rotating disc, *Proc. 33rd ASME Int. Gas Turbine Conf.*, Amsterdam, June (1988).
30. J. W. Chew, Predictions of flow in rotating disc systems using the k–ε turbulence model, Paper No. 84-GT-229, presented at the Gas Turbine Conf., American Society of Mechanical Engineers, Amsterdam, Holland (1984).
31. J. Fromm, A numerical study of unstable flow between rotating disks, IBM Res. Rept, RJ4734 (1985).
32. J. Fromm, Understanding turbulence through Navier–Stokes computation of flow between rotating disks, IBM Res. Rept, RJ5999 (1987).
33. G. K. Batchelor, Note on a class of solutions of the Navier–Stokes equations representing rotationally symmetric flow, *Q. J. Mech. Appl. Math.* **4**, 29–41 (1951).

34. K. Stewartson, On the flow between two rotating coaxial disks, *Proc. Camb. Phil. Soc.* **49**, 333–341 (1953).
35. M. Holodniok, M. Kubicek and V. Hlavacek, Computation of the flow between two rotating coaxial disks: multiplicity of steady-state solutions, *J. Fluid Mech.* **108**, 227–240 (1981).
36. A. Z. Szeri, A. Giron and S. J. Schneider, Flow between rotating disks (part 2. Stability), *J. Fluid Mech.* **134**, 133–154 (1983).
37. N. D. Nguyen, J. P. Ribault and P. Florent, Multiple solutions for flow between coaxial disks, *J. Fluid Mech.* **68**, 369–388 (1975).
38. C. E. Pearson, Numerical solutions for the time-dependent viscous flow between two rotating coaxial disks, *J. Fluid Mech.* **21**, 623–633 (1965).
39. G. L. Mellor, P. J. Chapple and V. K. Stokes, On the flow between a rotating and a stationary disk, *J. Fluid Mech.* **31**, 95–112 (1968).
40. P. LeQuere, J. A. C. Humphrey and F. S. Sherman, Numerical calculation of thermally-driven two-dimensional unsteady laminar flow in cavities of rectangular cross section, *Numer. Heat Transfer* **4**, 249–283 (1981).
41. B. E. Launder and C. H. Priddin, A comparison of some proposals for the mixing length near a wall, *Int. J. Heat Mass Transfer* **16**, 700–702 (1973).
42. S. V. Patankar, *Numerical Heat Transfer and Fluid Flow*. Hemisphere/McGraw-Hill, New York (1980).
43. B. P. Leonard, A stable and accurate convective modelling procedure based on quadratic upstream interpolation, *Comp. Meth. Appl. Mech. Engng* **19**, 59–98 (1979).
44. H. Tennekes and J. L. Lumley, *A First Course in Turbulence*. MIT Press, Cambridge, Massachusetts (1972).
45. C. J. Chang, Numerical calculations of laminar and turbulent flows and heat transfer in rotating-disk systems, Ph.D. Thesis, University of California at Berkeley (1989).

CALCUL DE LA CONVECTION TURBULENTE ENTRE DES DISQUES COROTATIFS DANS DES ENCEINTES AXISYMETRIQUES

Résumé—Une étude numérique est conduite pour un écoulement turbulent dans un espace non obturé entre une paire de disques bloqués sur le même arbre et une enceinte axisymétrique. La procédure aux différences finies (Chang *et al.*, *J. Heat Transfer* **111**, 625–632 (1989)) est étendue pour inclure un modèle de turbulence (k–ε) standard. Une relation de van Driest qui tient compte des effets de la courbure de l'écoulement et du cisaillement pariétal sur les échelles de longueur, est utilisé en conjunction avec l'hypothèse de longueur de mélange faite près de la paroi. Le système d'équations est résolu en supposant un écoulement à propriétés constantes, à symétrie circulaire et statistiquement permanent. Cette approche prédit des résultats de vitesse moyenne et de transfert thermique en bon accord avec les données expérimentales. Les prédictions révèlent un écoulement qui, en variables adimensionnelles, tend vers un état asymptotique limite aux grands nombres de Reynolds. En l'absence de soufflage, une paire symétrique de tourbillons transverses à l'écoulement apparait près de la paroi de l'enceinte et leur rotation augmente avec l'accroissement de la vitesse de rotation des disques. Des vitesses de rotation élevées, au dessus de 2400 tr min^{-1} dans la configuration étudiée, et des espacements faibles des disques, induisent de grandes valeurs de cisaillement et de température (dues à la dissipation visqueuse) au voisinage de la paroi de l'enceinte. L'écoulement et ses caractéristiques de transfert thermique peuvent être fortement altérés par les effets combinés de soufflage radial et axial. Spécifiquement, on montre que le soufflage axial réduit sensiblement le cisaillement et le transfert thermique à la paroi courbe de l'enceinte.

BERECHNUNG DER TURBULENTEN KONVEKTION ZWISCHEN GLEICHSINNIG ROTIERENDEN SCHEIBEN IN ACHSENSYMMETRISCHEN HOHLRÄUMEN

Zusammenfassung—Die turbulente Strömung im freien Raum zwischen zwei koaxialen, gleichsinnig rotierenden Scheiben in einem festen achsensymmetrischen Hohlraum wird numerisch untersucht. Das finite Differenzenverfahren nach Chang *et al.* (*J. Heat Transfer* **111**, 625–632 (1989)) wird um ein Standard-Zweigleichungs-(k–ε)-Turbulenzmodell für den Kernbereich der Strömung erweitert. Eine Beziehung nach van Driest, die den Einfluß der Stromlinienkrümmung auf die kennzeichnende Abmessung berücksichtigt, ist in Verbindung mit der Prandtl'schen Mischungsweghypothese angewandt worden, um die Strömung nahe der Wand nachzubilden. Das Gleichungssystem wurde unter den Annahmen konstanter Stoffeigenschaften sowie in Umfangsrichtung symmetrischer und quasistationärer Strömung gelöst. Die berechneten Werte für die mittlere Geschwindigkeit und den Wärmeübergang stimmen gut mit zeitgemittelten Versuchsdaten überein. Die Berechnungen ergeben für die Strömung bei Anwendung dimensionsloser Variabler einen Verlauf, der bei hohen Reynolds-Zahlen asymptotisch gegen einen begrenzenden Wert strebt. Ohne Einblasung ergibt sich ein symmetrisches quergerichtetes Wirbelpaar nahe der Hohlraumwand, dessen Rotationsgeschwindigkeit mit derjenigen der Scheiben ansteigt. Hohe Rotationsgeschwindigkeiten (bei der hier untersuchten Anordnung oberhalb von 2400 Umdrehungen pro Minute) und kleine Scheibenabstände führen zu großen Schubspannungen und Temperaturen in Wandnähe—dies wird durch die viskose Dissipation verursacht. Strömung und Wärmeübergang können sich durch radiale und axiale Einblasungen drastisch ändern. Insbesondere zeigt sich, daß eine axiale Einblasung Schubspannung und Wärmeübergang an der gekrümmten Hohlraumwand wesentlich reduziert.

РАСЧЕТ ТУРБУЛЕНТНОЙ КОНВЕКЦИИ МЕЖДУ ДИСКАМИ, ОДНОВРЕМЕННО ВРАЩАЮЩИМИСЯ В ОСЕСИММЕТРИЧНЫХ ПОЛОСТЯХ

Аннотация—Численно исследуется турбулентное течение в свободном пространстве между двумя закрепленными в центре соосными дисками, одновременно вращающимися в неподвижной осесимметричной полости. Метод конечных разностей (Chang *et al.* (*J. Heat Transfer* **111**, 625–632 (1989))) расширен включением стандартной двухпараметрической k–ε модели турбулентности в ядре потока. Соотношение ван Дриста, учитывающее влияние кривизны линий тока и сдвига у стенки на энергосодержащие масштабы длины, используется в сочетании с гипотезой Прандтля о длине смешения для моделирования пристенного течения. Система уравнений решается в предположении симметричного по окружности статистически стационарного течения с постоянными свойствами. Данный подход позволяет получить значения средней скорости и теплопереноса, которые хорошо согласуются с осредненными по времени экспериментальными данными. Приведенные в безразмерных переменных расчеты показывают, что течение при высоких значениях числа Рейнольдса стремится к предельному асимптотическому состоянию. В случае отсутствия вдува у стенки полости возникает симметричная пара вихрей, поперечных потоку, вращение которых увеличивается с ростом скорости вращения дисков. Высокие скорости вращения, превышающие в рассматриваемой конфигурации 2400 об мин$^{-1}$, и малые интервалы между дисками обусловливают большие значения сдвига и температуры (в силу вязкостной диссипации) вблизи стенки полости. Характеристики течения и теплопереноса могут существенно изменяться при совместном действии радиального и аксиального вдува. В частности, показано, что аксиальный вдув значительно уменьшает сдвиг и теплоперенос у изогнутой стенки полости.